Title
Temporal Regulation of Protein Assembly by Cdk1

Permalink
https://escholarship.org/uc/item/2q53f492

Author
Naylor, Stephen Gordon

Publication Date
2013

Peer reviewed|Thesis/dissertation

Temporal Regulation of Protein Assembly by Cdk1

by

Stephen Gordon Naylor

DISSERTATION

Submitted in partial satisfaction of the requirements for the degree of

DOCTOR OF PHILOSOPHY

in

BIOCHEMISTRY AND MOLECULAR BIOLOGY

in the

Copyright 2013

by

Stephen Gordon Naylor

ACKNOWLEDGEMENTS

Temporal Regulation of Protein Assembly by Cdk1

Stephen Gordon Naylor

ABSTRACT

Post-translational phosphorylation of proteins by cyclin-dependent kinases (Cdks) enables regulation of cell cycle events with a temporal and spatial precision that would be unattainable by control of protein synthesis and degradation alone. To understand how processes are regulated to operate reliably in every repetition of the cycle thus requires an understanding of where and when Cdk-dependent phosphates appear throughout the proteome, and the molecular effects of those phosphates on the proteins in question.

Cytokinesis, the process by which one cell divides and becomes two, involves the ordered assembly of several protein populations at the site of cell division. In the budding yeast *Saccharomyces cerevisiae*, this occurs at the bud neck and has the end result of coordinating the contraction of an actomyosin ring with the synthesis of the primary septum, a cell wall precursor. The assembly process occurs during a period or proteome-wide reversal of Cdk-dependent phosphorylation, and is known to be sensitive to perturbations of the Cdk regulatory system.

This study focuses on Iqg1, an essential protein required for recruiting actin to the bud neck. Iqg1 is phosphorylated by Cdk1 (*S. cerevisiae*'s sole essential Cdk) at several sites, and we find that mutation of these sites to yield a nonphosphorylatable Iqg1 disrupts the timing of several aspects of the pre-cytokinesis assembly process. When expressed in place of wild type Iqg1, the phosphomutant promotes early arrival of filamentous actin at the bud neck at levels comparable to those observed in response to

global inhibition of Cdk1 activity. In this mutant, we also observe early onset of the accumulation of Iqg1 itself, and of Hof1, a regulator of primary septum deposition that we reveal as a likely Iqg1 *in vivo* binding partner.

These results reveal a common point of regulation for the two processes that comprise cytokinesis and illuminate the relationships between proteins that govern the timing of assembly of a complex multi-protein apparatus. The quantitative fluorescence microscopy methods used also provide a system for the further study of the unique molecular consequences of phosphorylation for each of Cdk1's many protein substrates.

TABLE OF CONTENTS

LIST OF TABLES

LIST OF FIGURES

CHAPTER 1: INTRODUCTION

A major goal for basic research in the natural sciences is to unify the modes of understanding that have developed within the once-isolated disciplines of biology, chemistry and physics. For example, early chemists were able to define the phenomenon of the covalent bond, and to discover clear laws governing the creation and destruction of those bonds and the interactions among them. But only more recently have those discoveries gained real explanatory power through the efforts of modern scientists to describe these laws within the framework of more fundamental physical concepts such as elementary particles, waves and fields. Similarly, current studies in cell biology—a discipline born as the purely observational study of microscopic structures and movements—are largely focused on efforts to model complex interactions between macromolecules like proteins, nucleic acids and lipids in terms explainable by their underlying chemistry. A good cell biologist's work is never completed until the seemingly magical self-organization of components that happens within a living cell can be fully described and predicted in terms of cause and effect governed by basic electrostatic forces and free energy profiles.

Study of the cell division cycle provides an ideal opportunity to advance scientific understanding towards this goal. The cell cycle is the repeating and unidirectional set of phenomena that turn one cell into two copies of itself, each containing the full set of subcellular components that made up the parent cell. This process is essential to all cellular life, and the basic regulatory systems governing it are conserved among all eukaryotes[1]. Knowledge of the cell cycle enables the study of developmental biology, as it is modification of the primordial exact-copy program that creates multicellular life and

explains the growth of specialized tissues from stem cells. Cell cycle knowledge is also a crucial part of applied fields such as the study of cancers, diseases that are defined by the loss of proper cell cycle regulation within animal tissues. For the purposes of unifying biological and chemical understanding of the natural world, though, the most appealing reason to study the cell cycle is simply that it provides one of the most universal and immediately striking examples of the emergence of large-scale dynamic organization from random collisions of molecules. Watching through a microscope the exquisite condensation of DNA into tightly packed chromosomes, the coordinated segregation of those chromosomes to opposite ends of the cell that defines *mitosis*, and the furrowing and pinching movements known as *cytokinesis* that complete the transition from one cell to two, it is difficult not to imagine an overseeing puppet master pulling the strings from above. And yet the more we understand about the molecular components underlying these processes, the clearer it becomes that chemistry and physics among the small are fully sufficient to explain the orchestration of the large (well, larger).

The Central Dogma of Molecular Biology holds that a cell's DNA governs much of what goes on in a cell through the expression of protein molecules whose structure is encoded in the DNA's variable nitrogenous bases, organized into individual genes that encode individual proteins. The set of genes in a cell's DNA defines the parameters of that cell's potential, and the profile of which genes are being expressed—transcribed and translated into copies of protein—at a given time define what the cell is like at that moment. There is one set of genes being expressed while a cell is growing, another set being expressed while the cell is replicating its genome, and still another set being expressed during mitosis and cytokinesis. As a result, there is a distinct protein profile

inside the cell during each of these phases. One of the first major steps toward a molecular understanding of the eukaryotic cell cycle was the identification of several proteins called *cyclins* whose concentrations in the cell correlate tightly with the G1 (**G**ap), S (DNA **S**ynthesis) and M (**M**itosis/cytokinesis) phases defined by observational biology (Fig. 1). This correlation was soon shown to be a causal relationship, with cells unable to progress through the phases properly when cyclin concentrations were experimentally manipulated. That the mere presence of a single type of catalytically inert molecule in the cellular milieu is sufficient to control some of the most dramatic changes in a cell's life cycle was a revelation, but biology does not occur in a vacuum. A mass of DNA in an otherwise empty membrane will not undergo mitosis in response to injection of mitotic cyclin. Only through interactions with other proteins that have co-evolved to respond to a collision with the cyclins can the link between genetic information and physical phenomena be explained.

Two of the most remarkable aspects of the cell cycle are its irreversibility and its temporal precision. Naïvely, one might expect that simple variation in gene expression and consequent changes in protein concentration could explain these features. After all, whether a given gene is transcribed or not is itself under the control of proteins. It is not difficult to imagine a system wherein one gene expresses a protein that turns on expression of another gene, and so forth in a domino effect that, coupled with the natural degradation of existing proteins and the continual input of energy and material from food, could continue cyclically in perpetuity, never reversing direction or allowing phases to overlap. Indeed, such a system does constitute the core of the regulatory logic behind the cell cycle.

However, managing a cell cycle with only these tools would be a bit like cooking on electric stove coils, which is notoriously imprecise due to the delay between turning the knob and actually changing the temperature of the pan, with effects of the previous setting still going on the whole time. It takes time for a gene to be transcribed, edited, exported and translated into enough copies of protein to have its effect, and protein degradation times are variable and often not evolvable due to competing structural constraints inherent to the protein's function. Study of cell cycle events, in particular of the transitions between major phases, show them to be remarkably switch-like, with changes happening to completion on time scales that would be impossible by simply ramping gene expression up or down.

These switches are enabled by *post-translational modification* of proteins, chemical changes that take a protein from its native state to a new kind of molecule with distinct properties. Two of the most significant post-translational modifications in cell cycle regulation are *ubiquitination* and *phosphorylation*. Ubiquitin is a small protein that, when added in multiple copies to a protein's surface, marks that protein for immediate degradation by creating an affinity for the cell's garbage disposal, the proteasome[2]. The ability to rapidly destroy all copies of a given protein is crucial to the irreversibility of cell cycle transitions, and inquiry into the target selectivity, temporal control, and mechanism of action of the ubiquitin ligase enzymes behind this modification makes up a significant part of contemporary cell cycle research.

Phosphorylation is similar to ubiquitination in that it involves the covalent attachment of a molecule onto a protein's surface by a selective enzyme (known as a *kinase*), but the attached molecule in this case is a simple phosphate group (PO_4^{2-}) rather than a whole

protein, and the effects are much more diverse than a simple tag for destruction. Phosphorylation also turns out to be the mechanism by which cyclins affect the behavior of other proteins. Cyclins are ineffectual except upon binding to a cyclin-dependent kinase (Cdk) enzyme. The cyclin-Cdk pair catalyzes a chemical reaction between free ATP and a nucleophilic side chain on the target protein's surface, resulting in a phosphorylated form of the protein (Fig. 2). Opposing enzymes called *phosphatases* return phosphorylated proteins to their native state by catalyzing a hydrolytic reaction that clips the phosphate from the protein's surface. The balance between kinase and phosphatase activities gives the cell the opportunity to change the cell's protein profile in a rapid and finely tuned way far beyond what would be possible relying on the wholesale creation and destruction of proteins. Cdks phosphorylate a huge number of protein substrates; in the budding yeast *Saccharomyces cerevisiae*, roughly 600 of the organism's 6000 protein types are thought to be Cdk substrates. Understanding the causal power of cellular cyclin concentrations thus begins with understanding how each protein substrate responds to the addition or removal of Cdk-dependent phosphates.

From an information theory perspective, the post-translational phosphate modification can be thought of as a marker, a binary yes/no switch on a protein whose meaning is translated by the protein's binding partners into a change in that protein's function. Indeed, examples abound of enzymes for which being phosphorylated or dephosphorylated at a single site serves as an on/off switch for catalytic activity, or protein-protein interactions that are completely abolished when one partner is phosphorylated. From this perspective, the chemical identity of the marker might be considered arbitrary, just a way of making a protein different in some identifiable way.

However, from the perspective of a scientist wishing to bridge the biology-chemistry divide, the use of phosphate is of particular interest. The phosphate group has remarkable properties within the realm of organic chemistry. The ester bond that links the group to other molecules is unusual in being highly unstable thermodynamically, yet highly persistent kinetically. Because of this, phosphate bonds play a key role in many of biology's most fundamental systems. The phosphodiester bonds in ATP provide a portable and versatile form of chemical energy and have thus enabled the evolution of ATP as the primary energetic currency of all life. The phosphate-based backbone of DNA creates a polymer that is stable enough to reliably maintain vital genetic information over a cell's lifetime, while also being able to self-assemble with the extreme rapidity necessary to facilitate DNA replication, the central feature of life as we know it as a self-copying chemical phenomenon. In the biochemistry of metabolism, the cell also reversibly phosphorylates carbohydrates as a way to keep the respiration process that converts food into usable energy moving in the correct direction and within the correct subcellular compartments. It is no surprise that the same chemistry would be employed to create a rapidly reversible and highly versatile way of regulating protein activity throughout the cell cycle.

The high negative charge of a phosphate group provides a great opportunity to form hypotheses about exactly how, on a chemical level, the post-translational modification of a protein can influence the large-scale organization of cellular phenomena, which are after all the emergent properties of electrostatic interactions between positively and negatively charged subatomic particles. Learning all we can about how the distribution of post-translational phosphates across the proteome is determined, and how each targeted

protein is changed by the modification, is an essential part of the task of demystifying biological phenomena and creating a more unified and predictive scientific understanding of the natural world.
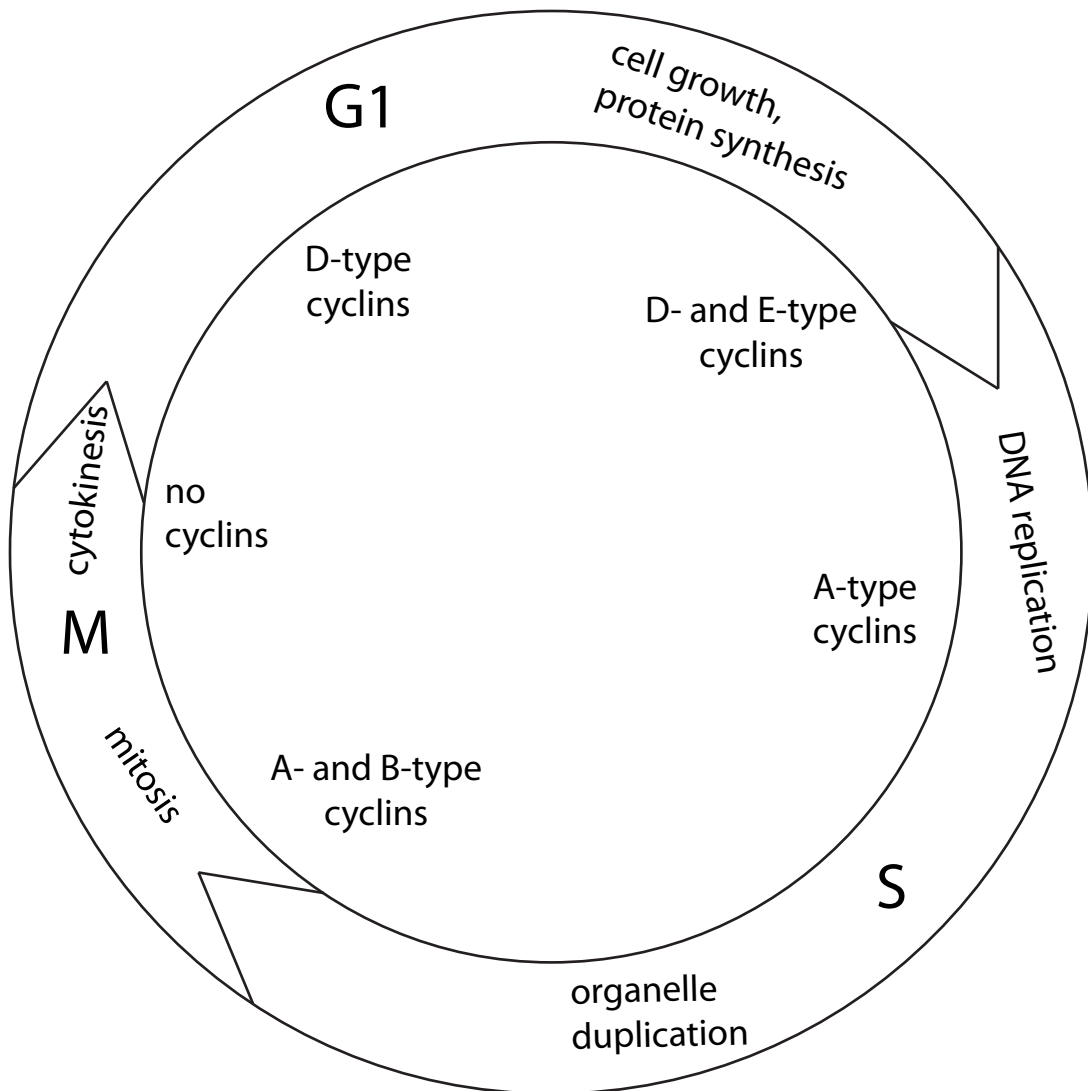
Figure 1: Cyclin concentrations correlate with cell cycle phases and activities
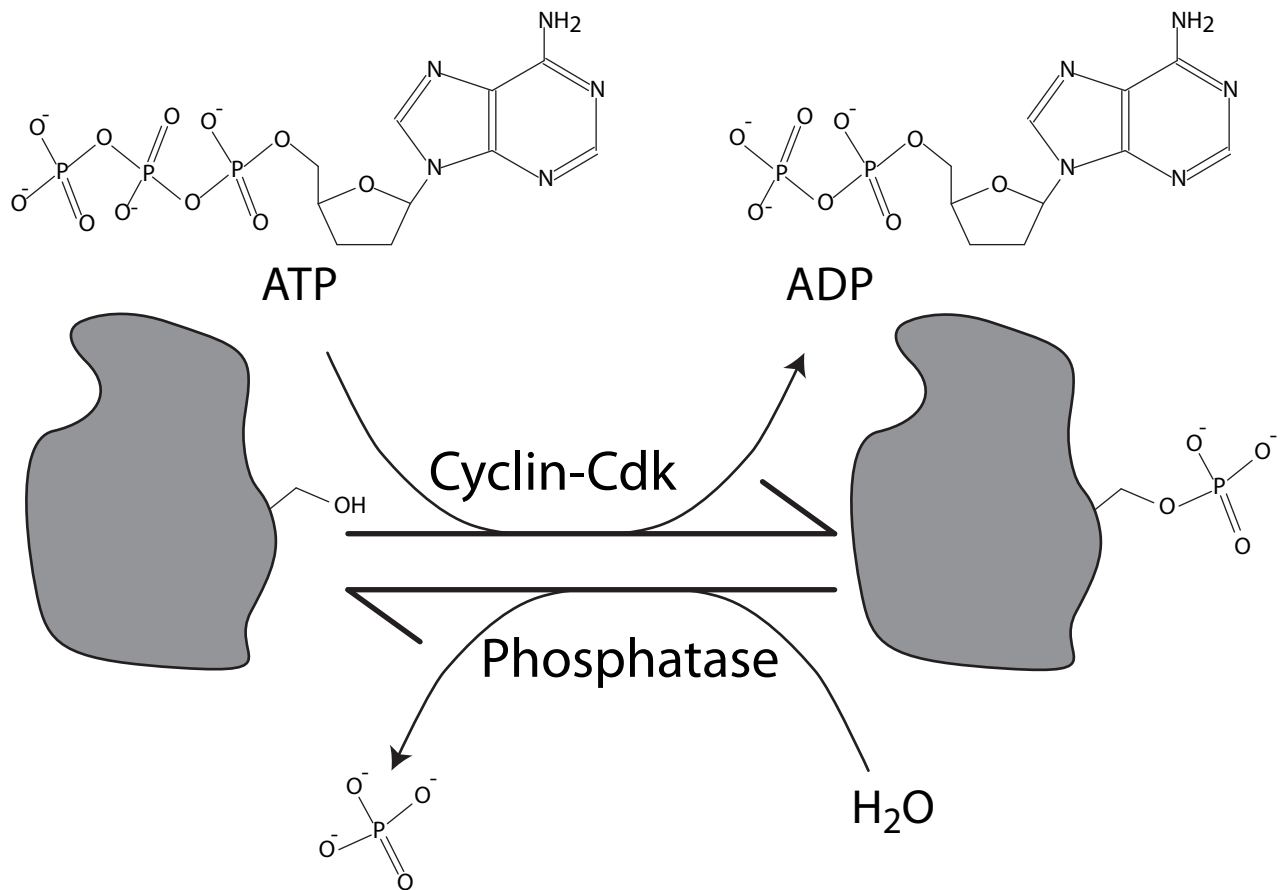
Figure 2: Chemistry of post-translational protein phosphorylation

Cyclin-Cdk complexes catalyze transfer of phosphate from ATP to protein surface using energy from ATP phosphodiester bond. Phosphatases catalyze return of protein to native state using energy from protein-phosphate bond.

CHAPTER 2: Cdk1-DEPENDENT PHOSPHORYLATION OF Iqg1 GOVERNS ACTOMYOSIN RING ASSEMBLY PRIOR TO CYTOKINESIS

This chapter has been submitted to the Journal of Cell Biology on August 12, 2013.

Abstract

Contraction of the actomyosin ring (AMR) provides the centripetal force that drives cytokinesis. In budding yeast, assembly and contraction of the AMR is coordinated with membrane deposition and septum formation at the bud neck. A central player in this process is Iqg1, which promotes recruitment of actin to the myosin ring and links AMR assembly with that of the septation apparatus. We observe early actin recruitment in response to inhibition of cyclin-dependent kinase 1 (Cdk1) activity, and we find that the Cdk1-dependent phosphorylation state of Iqg1 is a determining factor in the timing of bud neck localization of both Iqg1 and actin, with both proteins accumulating prematurely in cells expressing nonphosphorylatable Iqg1 mutants. Hof1, a regulator of primary septum deposition, also appears early at the bud neck in these mutants, providing a regulatory link between the septation and contractile pathways that cooperate to complete cytokinesis.

Introduction

Cytokinesis requires the spatial and temporal regulation of multiple components at the site of cell division. In animal and fungal cells, a ring of actin filaments and myosin forms inside the plasma membrane [3, 4]. As myosin motor activity contracts the ring and draws the membrane inward, new plasma membrane and extracellular matrix are deposited at the division site. The cell must coordinate these processes with each other and relative to other cell cycle events to ensure that cell division occurs only after completion of mitosis.

In the budding yeast, *Saccharomyces cerevisiae*, cytokinesis is carried out by structures and processes homologous to those in animal cells [5], including a contractile actomyosin ring (AMR) [6] and a cell wall deposition pathway with similarities to mammalian extracellular matrix remodeling [7]. However, the budding yeast life cycle, with its "pre-furrowed" division site, enables perturbation of either process without lethal effects [8-10], making *S. cerevisiae* a valuable model for study of the regulatory relationships among the proteins involved.

The yeast AMR is assembled throughout the cell cycle [8], beginning in G1 with the accumulation of septin proteins at the bud site [11, 12]. A septin-dependent ring of the type-II myosin heavy chain, Myo1, forms at the nascent bud neck. Next, the septin-binding protein Bni5 [13] and the formins Bnr1 and Bni1 [14] arrive at and depart from the bud neck, interacting with the Myo1 tail to guide Myo1 into its final position [15]. The myosin light chain protein Mlc1 arrives in mitosis [16] and facilitates recruitment of the protein Iqg1 [17],

which stabilizes the Myo1 ring [15] and is required for the recruitment of filamentous actin (f-actin), which completes AMR assembly [8, 18, 19].

AMR contraction is coupled with the onset of cell wall formation, which begins with the centripetal deposition of the primary septum (PS) by chitin synthase II (Chs2) [20, 21]. A secondary septum (SS) is then deposited along the PS and becomes the cell wall upon digestion of the PS. Like AMR assembly, PS deposition follows the sequential bud neck localization of several proteins, most importantly Hof1, Cyk3 and Inn1 [22-26].

While disruption of AMR contraction and PS deposition together is lethal [14], neither process alone is essential for viability [6, 8-10]. However, each process is defective in the absence of the other, as *myo1*Δ cells deposit a misoriented PS [9, 15] and *chs2*Δ cells produce unstable and asymmetric AMRs [10, 27]. The two processes are at once physically distinct, mutually interdependent and partially redundant, a relationship that invites and facilitates more detailed molecular investigation. Genetic studies have illuminated the dependencies underlying sequential protein recruitment to the bud neck [28-30], but the temporal regulation of these components remains unclear.

The 173 kDa protein Iqg1 is one of the few cytokinesis components that is essential for viability [18]. Homologous to the mammalian IQGAP proteins that bundle f-actin [31, 32] and regulate actin-dependent processes [33, 34], Iqg1 is required for actin recruitment to the bud neck [6, 8, 18] and interacts genetically with PS regulators such as Cyk3 [24]. Its large size and multi-domain architecture, together with its essential function, make Iqg1 a likely physical link between the AMR and PS machinery.

Cytokinesis occurs during a period defined by the inactivation of cyclin-dependent kinase 1 (Cdk1) and the dephosphorylation of Cdk1 protein substrates, brought on by

mitotic cyclin degradation and Cdc14 phosphatase activation [35]. Dephosphorylation of

Cdk1 substrates underlies many events of late mitosis and cytokinesis [36, 37, 38-40, 41].

Similarly, the mitotic exit network (MEN) that sustains Cdc14 activity regulates septin

dynamics [42, 43], actin localization [44], PS function [30], and AMR contraction [14, 43, 45].

We addressed the mechanisms by which Cdk1 substrate dephosphorylation governs

AMR assembly and contraction. We identified Cdk1 phosphorylation of Iqg1 as a

mechanism for controlling the AMR assembly and PS deposition pathways, providing

insight into the mechanisms by which Cdks control the timing and coordination of

cytokinetic events.

Results and discussion

Inhibition of Cdk1 is sufficient for pre-anaphase recruitment of f-actin to the bud neck

Chemical inhibition of Cdk1 in mammalian cells can induce premature cytokinesis [46]. We

therefore hypothesized that Cdk1 inhibition in yeast can trigger premature cytokinetic

processes such as AMR assembly. We used confocal fluorescence microscopy in

combination with an analog-sensitive allele of *CDK1* (*cdk1-as*) that is specifically

inhibited by the purine analog 1-NM-PP1[47]. Wild-type and *cdk1-as* cells were arrested in

a metaphase state by nocodazole treatment, and 1-NM-PP1 was added for 15 minutes.

Cells were then fixed and stained with fluorophore-conjugated phalloidin to visualize f-

actin structures. A ring of f-actin at the bud neck, indicating a prematurely assembled

AMR, was clearly visible in only about 7% of wild-type cells arrested in metaphase. This

number rose to 27% in mock-treated *cdk1-as* cells, and 73% when treated with 1-NM-

PP1 (Fig. 1 A, B). Thus, Cdk1 inhibition results in premature actin ring assembly. The

partial phenotype in the absence of inhibitor is consistent with previous evidence that

Cdk1-as is a moderately weakened kinase[47].

Cells expressing nonphosphorylatable Iqg1 assemble a pre-anaphase actin ring

We set out to identify Cdk1 substrates whose dephosphorylation is sufficient to reproduce

the effects of Cdk1 inhibition on AMR assembly. Iqg1 was an appealing candidate, due

to its essential role in AMR assembly and because it contains 20 sites matching the

minimal Cdk1 recognition motif (S/T-P), 7 of which are known to be phosphorylated in

mitotic cells and rapidly dephosphorylated after Cdk1 inhibition[48] (Fig. 2 A). Cdk

phosphorylation of an Iqg1 ortholog also regulates AMR assembly in the yeast *Candida*

albicans[49]. Iqg1 contains multiple functional domains, including an APC/C recognition

sequence[50, 51], a calponin homology domain (CHD) required for actin recruitment and

homologous to known mammalian actin-bundling domains[52], several IQ repeats that

localize Iqg1 to the bud neck through an interaction with Mlc1[17], and a degenerate GAP-

related domain (GRD) associated with AMR contraction[19]. The 20 Cdk consensus sites

occur in three clusters: 3 sites near the N-terminal APC/C recognition sequence, 11 sites

between the CHD and the IQ-repeat region, and 6 sites within the GRD near the C-

terminus (Fig. 2 A).

We analyzed the functions of these clusters individually and in combination by

introducing mutant alleles of *IQG1* at its endogenous locus. Serines or threonines were

replaced with alanines to generate the alleles *iqg1-3A, iqg1-11A, iqg1-6A,* and *iqg1-14A*

(*11A* and *3A* in combination) (Fig. 2 A and Tables S1, S2). All mutants proliferated at

normal rates under nutrient-rich conditions (Fig. 2 B). After two hours of nocodazole

treatment, the *iqg1-3A*, *-11A*, and *-14A* populations showed clear f-actin rings in a majority of metaphase-arrested cells, compared to only 9% for wild-type *IQG1* (Fig. 2 C-D). The *iqg1-14A* actin ring frequency did not differ significantly from that observed in our earlier experiments with Cdk1-as inhibition, suggesting that dephosphorylation of Iqg1 is sufficient to explain the Cdk1 inhibition phenotype. *iqg1-6A* displayed no difference from wild type in this and other experiments (Fig. 2 C-D, and data not shown), so the six C-terminal sites were excluded from further analysis.

To assess the timing of AMR assembly in an unperturbed cell cycle, we measured the frequency of f-actin rings in an asynchronous, exponentially-growing culture (Fig. 3 A). The spindle pole body (SPB)-associated protein Spc42 was tagged with the red fluorescent protein mCherry, permitting the sorting of cells into three cell cycle stages based on SPB spacing. The proportion of cells in each stage was not significantly altered in any mutant, suggesting no overall defect in cell cycle progression (Fig. 3 B). Actin rings were not observed in G1 or S-phase cells with single or unseparated SPBs (data not shown). In wild-type cells, rings were observed only in cells whose wide SPB spacing indicated an elongated anaphase spindle, and even then in only 52% of cells (Fig. 3 A, C). By contrast, *iqg1-14A* populations displayed f-actin rings in 27% of cells with short pre-anaphase spindles and in 74% of cells with anaphase spindles (Fig. 3 A, C). *iqg1-3A* and *-11A* populations showed similar but slightly lower ring frequencies than the *iqg1-14A* combination. Thus, f-actin recruitment to the AMR occurs only after the initiation of spindle elongation in wild-type cells, but prior to anaphase in the Iqg1 phosphomutants.

These observations, combined with those of nocodazole-arrested mutants in which AMRs persist without contraction, demonstrate that the colocalization of actin and

myosin is not sufficient for contraction. Stable AMRs incompetent for contraction have been described previously in the case of an *iqg1* mutant lacking the GRD[19]. Our observations further suggest that AMR assembly and contraction are controlled separately.

Nonphosphorylatable Iqg1 arrives at the bud neck prematurely

The premature recruitment of f-actin to the bud neck in *IQG1* phosphomutants might be explained by an increase in binding affinity between Iqg1 and f-actin, or by premature localization of Iqg1 itself, or by a combination of both. We explored these possibilities by tagging Iqg1 with enhanced green fluorescent protein (eGFP) and measuring Iqg1-eGFP dynamics over the cell cycle in live cells by time-lapse microscopy, again using Spc42-mCherry as a marker for cell cycle progression (Fig. 4 A).

The *iqg1* phosphomutants matched wild-type cells in measures of overall cell cycle duration and time between major SPB dynamics milestones (data not shown). However, the behavior of Iqg1-eGFP in relation to those milestones was altered dramatically. A ring-shaped fluorescence signal became visible 4-8 minutes after the onset of spindle elongation in a typical *IQG1-eGFP* cell but 15-20 minutes prior to elongation onset in a typical *iqg1-14A-eGFP* cell (Fig. 4 A, C).

To obtain a more quantitative understanding, we measured the mean fluorescence per pixel within the bud neck region. The results confirmed early Iqg1-eGFP accumulation in the phosphomutant relative to onset of spindle elongation (Fig. 4 B, D). Results for *iqg1-11A* did not differ significantly from those for *iqg1-14A*, while *iqg1-3A* yielded a less severe phenotype (Fig. 4 E), as in our studies of actin localization (Fig. 3 C). The timing

of peak Iqg1-eGFP concentration was not affected, suggesting that the full recruitment of Iqg1 depends on additional factors. Considering the actin results presented above, this suggests that sub-peak levels of dephosphorylated Iqg1 at the bud neck are sufficient for f-actin recruitment. Iqg1 ring contraction and degradation proceeded with wild-type timing in all strains (data not shown).

PS deposition regulator Hof1 binds Iqg1 and localizes to the bud neck prematurely in cells expressing nonphosphorylatable Iqg1

Based on the premature localization of Iqg1 phosphomutants, we hypothesized that Cdk1 phosphorylation weakens the binding affinity between Iqg1 and proteins that recruit Iqg1 to the bud neck. Previous studies identified Mlc1 as a binding partner of Iqg1 whose localization profile matches that of the hypothesized recruiter[16, 17]. To test the possibility that Iqg1 phosphorylation inhibits interactions with its binding partners, we analyzed Iqg1-associated proteins in immunoprecipitates of Iqg1-eGFP from nocodazole-arrested cells. Gel analysis (Fig. 5 A) revealed specific binding of Iqg1-eGFP and several proteins, including a 16 kDa protein near 1:1 stoichiometry to Iqg1-eGFP. Mass spectrometry identified this protein as Mlc1 (Table S3 A). We did not observe reproducible differences in Mlc1 band intensity between the wild type and *iqg1-14A* immunoprecipitates. We note, however, that microscopic analysis of insoluble lysate fractions revealed many intact Iqg1-eGFP rings, so the interactions analyzed in this experiment may be limited to soluble Iqg1-Mlc1 complexes that were not incorporated into the AMR.

Mass spectrometry identified the second most prominent Iqg1-associated protein as the F-BAR protein Hof1 (Table S3 B), a bud neck protein that regulates primary septum

deposition through interactions with Inn1 and Chs2[26, 53]. The heretofore-undescribed interaction between Iqg1 and Hof1 led us to hypothesize that Iqg1 phosphorylation influences Hof1 localization and thereby links the AMR and septum deposition pathways. To explore this possibility, we analyzed Hof1-eGFP dynamics in relation to spindle elongation in *IQG1* or *iqg1-14A* cells. While Hof1-eGFP generally accumulated at the bud neck earlier and more gradually than Iqg1-eGFP (Fig. 5 B, C), *iqg1-14A* cells initiated Hof1-eGFP accumulation slightly earlier than wild-type (Fig. 5 B). Statistical significance was demonstrated by marking the time at which each bud neck exceeded half-maximal eGFP fluorescence: 14% of the counted *iqg1-14A* cells accumulated more than half of their bud neck Hof1 before the onset of spindle elongation, compared to less than 2% of *IQG1* cells (Fig. 5 D). *iqg1-11A* yielded a similar distribution to *iqg1-14A*, while *iqg1-3A* again displayed an intermediate phenotype (10% of cells) (data not shown). We conclude that phosphorylation of Iqg1 helps control the recruitment of Hof1 to the bud neck.

Cdk1 coordinates AMR function and septation through Iqg1

The processes of AMR contraction and PS deposition are partially redundant and mutually interdependent[14, 54]. Iqg1 is essential for both processes. This study demonstrates that the expression of nonphosphorylatable Iqg1 is sufficient to accelerate the assembly of both the AMR and PS-depositing complexes, identifying Iqg1 as a key physical and regulatory link that helps provide the tight temporal coordination between the two processes.

While *iqg1* phosphomutants begin assembling Iqg1, Hof1 and actin at the bud neck prematurely, they reach full Iqg1 concentrations and undergo AMR contraction with wild-type timing, suggesting an additional regulatory trigger needed for completion of cytokinesis. Dephosphorylation of additional Cdk1 substrates could serve this role. The SH3-domain protein Cyk3 arrives at the bud neck just prior to AMR contraction and is involved in interactions with Hof1 and Inn1 that lead to activation of chitin synthesis by Chs2[26][29]. We found that Cyk3 and Inn1 localize normally in *iqg1-14A* cells (Fig. S1 A-B). Cyk3 is also a Cdk1 substrate[48], so an intriguing possibility is that Cdk1 phosphorylation of Cyk3 helps govern later steps in cytokinesis.

Our studies raise the question of how phosphorylation affects Iqg1 at the molecular level. Since the effect of phosphorylation on AMR assembly is inhibitory, the simplest possibility is that phosphorylation disrupts an interaction between Iqg1 and other proteins. Alternatively, the inhibition of Iqg1 bud neck localization could involve phosphate-dependent binding to a third-party protein that competes with the bud neck for Iqg1 binding. Iqg1 might also inhibit its own recruitment if phosphorylation causes the protein to fold so as to obscure a binding site. Such models are appealing because none of the key phosphosites fall within the IQ repeat region known to be responsible for Iqg1 localization.

The persistence of the phenotype in both the *iqg1-3A* and *iqg1-11A* mutants (albeit to different degrees) supports the possibility that Iqg1 must be phosphorylated at two distant regions to inhibit AMR assembly. This might be explained by Iqg1 binding to its recruiter(s) via multiple surfaces or by a folding structure wherein the two regions form a single binding surface. Another possibility is a kinase priming mechanism, wherein

phosphorylation of one site promotes phosphorylation of other sites to produce a downstream effect.

The stoichiometric relationship observed between Iqg1 and Mlc1 in our co-immunoprecipitation analysis suggests that Iqg1 might arrive at the bud neck as part of a soluble complex, expanding the possibilities for the mechanistic impact of phosphorylation. Further analysis of Iqg1 binding partners and the timing of their interactions should be combined with structural studies and the investigation of other phosphoproteins such as Cyk3, to more fully understand the regulatory circuits that enable the robust and timely coordination of multiple complex processes during the final stage of cell reproduction.

Materials and methods

Yeast procedures

Yeast strains were made in the W303 strain background and are listed in Table S1. Cultures were grown at 30°C in YEP + 2% D-glucose, except where noted. To achieve mitotic arrest, 15 µg/ml nocodazole was added to a mid-log-phase culture for 2 h. For Cdk1 inhibition, 10 µM 1-NM-PP1 was added for an additional 15 min following nocodazole treatment.

Plasmid construction and mutagenesis

Plasmids are listed in Table S2. To create pSGN092, PCR-amplified full-length *IQG1*, including all 5' and 3' untranslated regions, was subcloned into the pRS306

integrating plasmid. Synthetic fragments of *iqg1* alanine mutants (Invitrogen LifeTech gene synthesis) were subcloned into the pSGN092 backbone to generate plasmids containing full-length *iqg1* phosphomutant alleles.

For endogenous genomic replacement of *IQG1*, PCR from these plasmids amplified the 5' half of *iqg1* along with a *URA3* selection cassette and a homology region to promote insertion at the *IQG1* locus. Transformation of wild-type yeast with these PCR products and sequential selection for and then against the *URA3* marker left the genomic locus unchanged aside from the alanine mutations and two introduced restriction sites that do not affect amino acid sequence. A wild-type control strain underwent parallel transformations using wild-type plasmid (pSGN092) as PCR template. The C-terminal mutant, *iqg1-6A*, was made separately by integration of the full pSGN094 plasmid, followed by a similar selection/counterselection process. In all cases, mutagenesis was verified by PCR and sequencing of the full *IQG1* locus.

To construct C-terminal molecular fusions, we used PCR from pYM28 (eGFP, *HIS3* selection) or pSGN099 (mCherry, *kanMX* selection), with primers to target genomic insertion in place of the gene's stop codon. Transformants were verified by PCR and by fluorescence microscopy.

Visualization of f-actin

Cells were fixed by mixing 1.35 ml culture ($OD_{600} = 0.4 - 0.6$) and 150 µl of 37% formaldehyde (FA at room temperature for 10 min. All subsequent reagents were in 0.1 M KH_2PO_4/K_2HPO_4 buffer at pH 7.0, and all centrifugation steps are 5 min at 1000x*g* at room temperature. Cells were washed by centrifugation, resuspended in 3.7% FA, and

mixed for 1 of 16 h at 4°C. Cells were washed, treated with 10 mM ethanolamine to quench FA, briefly sonicated to separate cell clusters, permeabilzed with 0.2% Triton X-100 for 15 min, and incubated for 45 min in 60 µl of 0.2% Triton X-100 + 3 U/ml of Alexa 488-conjugated phalloidin (Invitrogen Molecular Probes), agitating periodically to keep cells in suspension. Cells were mounted on concanavalin-A-coated coverslips in Vectashield mounting medium (Vector Laboratories) containing 1 µg/ml DAPI, and imaged within hours by spinning disk confocal microscopy in the Nikon Imaging Center at UCSF.

Microscopy

For phalloidin experiments, samples were illuminated by 491 nm and 561 nm lasers and images were captured as stacks of 19 Z-planes spaced 0.4 µm apart, each 512 x 512 pixels (10.6 px/µm), using a 100x objective under the control of µManager software[55] (Microscope: Nikon Ti; Spinning Disk Confocal: Yokogawa CSU-22; Camera: Photometrics Evolve EMCCD). Cells were analyzed by comparison of a Z-projected (by maximum value) single image with the slice-by-slice three-dimensional data for each field of view. Only bud necks that showed both a clear horizontal band across the bud neck in the projected image and a curved pattern of staining that traced the plasma membrane in the 3D data were scored as f-actin rings. In nocodazole experiments, cells that lacked a single DAPI mass and symmetrical actin membrane patch distribution (10-20% of total) were not counted as arrested cells.

For eGFP experiments, mid-log-phase cells in synthetic complete media + 2% D-glucose (SD) were harvested by centrifugation and sealed between a coverslip and a 20

mm x 20 mm pad of recently-cast 1% agarose in SD. Microscopy was performed as above, except using a 60x objective and 10 Z-planes spaced 0.6 μm apart every 40 s for 2 h over five nearly-adjacent viewfields, each 512 x 512 pixels (6.4 px/μm).

For quantitative analysis of eGFP-tagged proteins in live cells, average-value Z-projections were stack-registered to compensate for drift in field of view, and a single time-projected image was created by taking the maximum-value signal across all 180 time points for each pixel. Regions of interest (bud necks) were defined based on this time-projected image, and average eGFP signal intensity within each region was measured for each time point in the average-Z-projected image. Data for each bud neck was normalized vertically such that mean fluorescence value ranged from 0 to 1 over the time course.

The time point corresponding to onset of spindle elongation was defined as the time when SPBs moved apart from each other and continued to move apart in subsequent time points.

For Hof1-eGFP data, time points corresponding to half-maximal fluorescence were determined by smoothing each cell's normalized data (reporting fluorescence value at each time point as the rolling average of the nearest four time points), then identifying the first time point reported as greater than 0.5.

Immunopurification of Iqg1-eGFP

1.5 L of nocodazole-arrested cultures were chilled on ice for 20 min, harvested by centrifugation, washed with chilled IP buffer (10 mM Tris-HCl pH 7.5, 150 mM NaCl, 0.5 mM EDTA), dripped directly into liquid Nitrogen, and stored at -80°C. 9 g pellets

were ground into fine powder by cryo-grinding (Retsch MM301 Ball Mill, 3 x 3 min, 30

Hz). Powder was resuspended in 12 ml IP buffer plus protease and phosphatase inhibitors

and lysis completed by 4 x 30 s blending with a tissue homogenizer (Polytron PT 1200

E). The soluble fraction was isolated following 1 h of ultracentrifugation (50,000 rpm at

4°C), and incubated for 4 h at 4°C with 35 µl of sepharose bead slurry coated with

monoclonal GFP-Trap antibody (Chromotek, Allele Biotech) for 4 h at 4°C. Beads were

collected by light centrifugation, washed three times, resuspended in 40 µl SDS-PAGE

buffer (20 mM Tris-HCl pH 6.8, 2% SDS, 4% glycerol, 10 mM β-mercaptoethanol) and

boiled for 60 s. 15 µl of supernatant was analyzed on a 4-12% gradient SDS-PAGE gel

and stained with Sypro-Ruby (Invitrogen) or GelCode Blue Stain (Thermo Scientific)

Mass Spectrometry

Protein bands or lane fragments were in-gel digested according to a published protocol

(http://msf.ucsf.edu/ingel.html). Briefly, SDS and chemicals used for staining/destaining

were removed with 20 mM ammonium bicarbonate buffer in 50% acetonitrile/water.

Disulfide bonds were reduced with DTT, and free sulfhydryls were alkylated with

iodoacetamide. Reagent excess was removed with the above buffer, and proteins were

incubated with side-chain protected porcine trypsin (Promega, Madison, WI) overnight at

37°C. The resulting peptides were extracted with 5% formic acid in 50%

acetonitrile/water and fractionated by reversed-phase chromatography on a C18 column

(75µmx150 mm) with gradient elution (starting with 2% B up to 35% B in 35 min;

solvent A: 0.1% formic acid in water; solvent B: 0.1% formic acid in acetonitrile; flow

rate: 600 nL/min) using a nanoACQUITY uHPLC system (Waters, Milford, MA) directly

linked to a linear ion trap – Orbitrap hybrid tandem mass spectrometer (LTQ-Orbitrap XL, Thermo Fisher Scientific, San Jose, CA). The six most abundant multiply-charged ions of each MS survey were automatically selected for CID analysis. The precursor masses were measured in the Orbitrap and CID data were acquired in the linear ion trap. Dynamic exclusion was enabled. In-house software (PAVA) was used for peak list generation. Database search was conducted using Protein Prospector 5.10.10, against the SwissProt database, downloaded March 21st 2013. *Saccharomyces*, *Homo sapiens*, *Bos taurus*, *Sus scrofa* proteins and the GFP sequence were searched (35417/535248 entries searched).

Online Supplemental Material

Fig. S1 shows live-cell eGFP analysis of the bud neck proteins Cyk3 and Inn1. Tables S1 and S2 describe yeast strains and plasmids used in this study. Table S3 provides full mass spectrometric analysis of bands identified in Fig. 5A.

26

A

+ DMSO + 1-NM-PP1

CDK1

cdk1-as

B
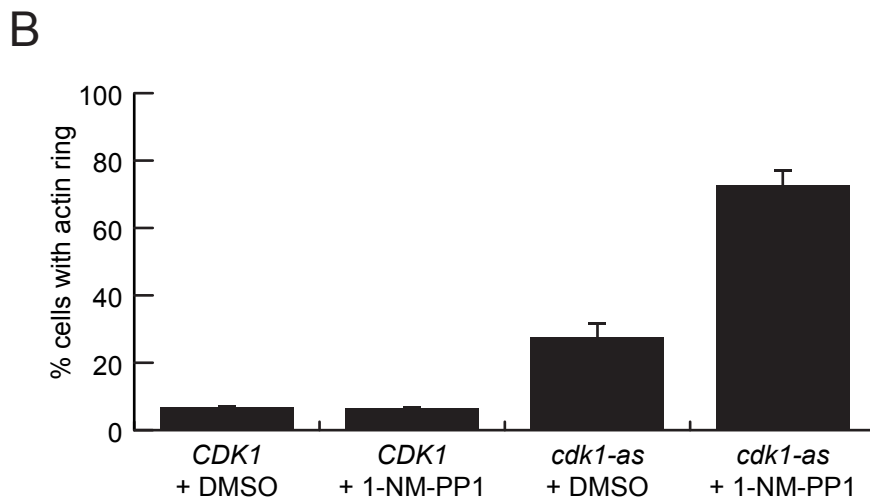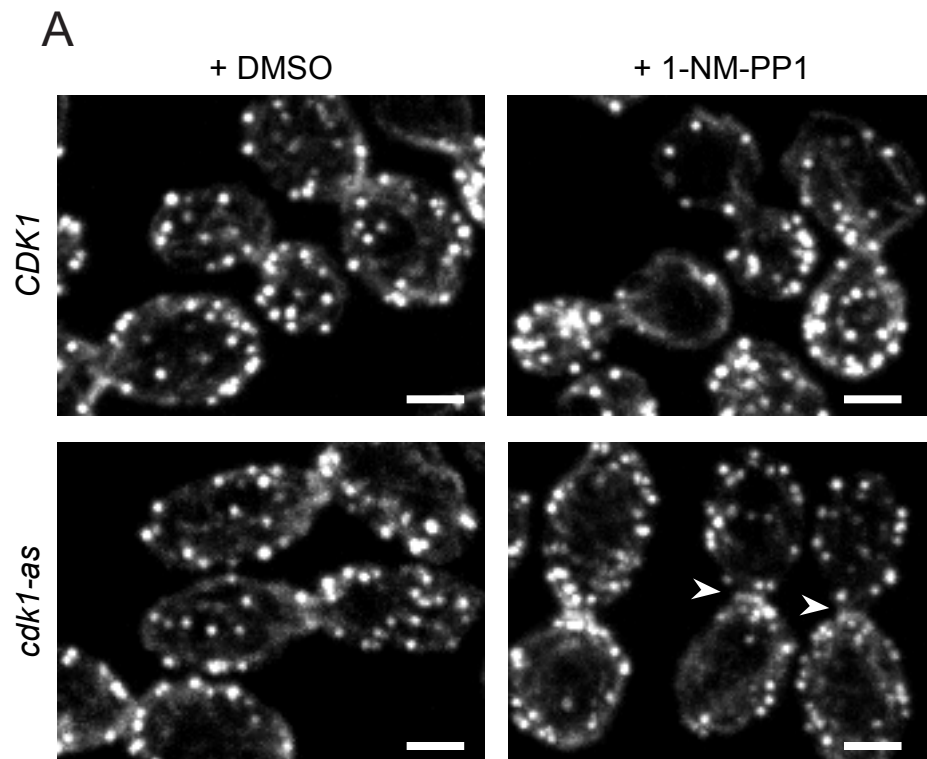
FIGURE 1

Actin ring assembly in response to Cdk1 inhibition. (A) Phalloidin-stained f-actin in nocodazole-arrested cells treated with 10 µM 1-NM-PP1 or DMSO for 15 min. Arrowheads: f-actin rings. Scale bars: 2 µm. (B) Actin ring frequency in nocodazole-arrested cells. Error bars: SEM in three experimental repeats.

A

‘3A’ Cluster ‘11A’ Cluster ‘6A’ Cluster

SPSK...TP...SP   TP....SP....TPRK..TPSP..TP..TP..SPIK..SP....SP..SPMR   SP..SP..SP..SPSP..SP

B

C

D
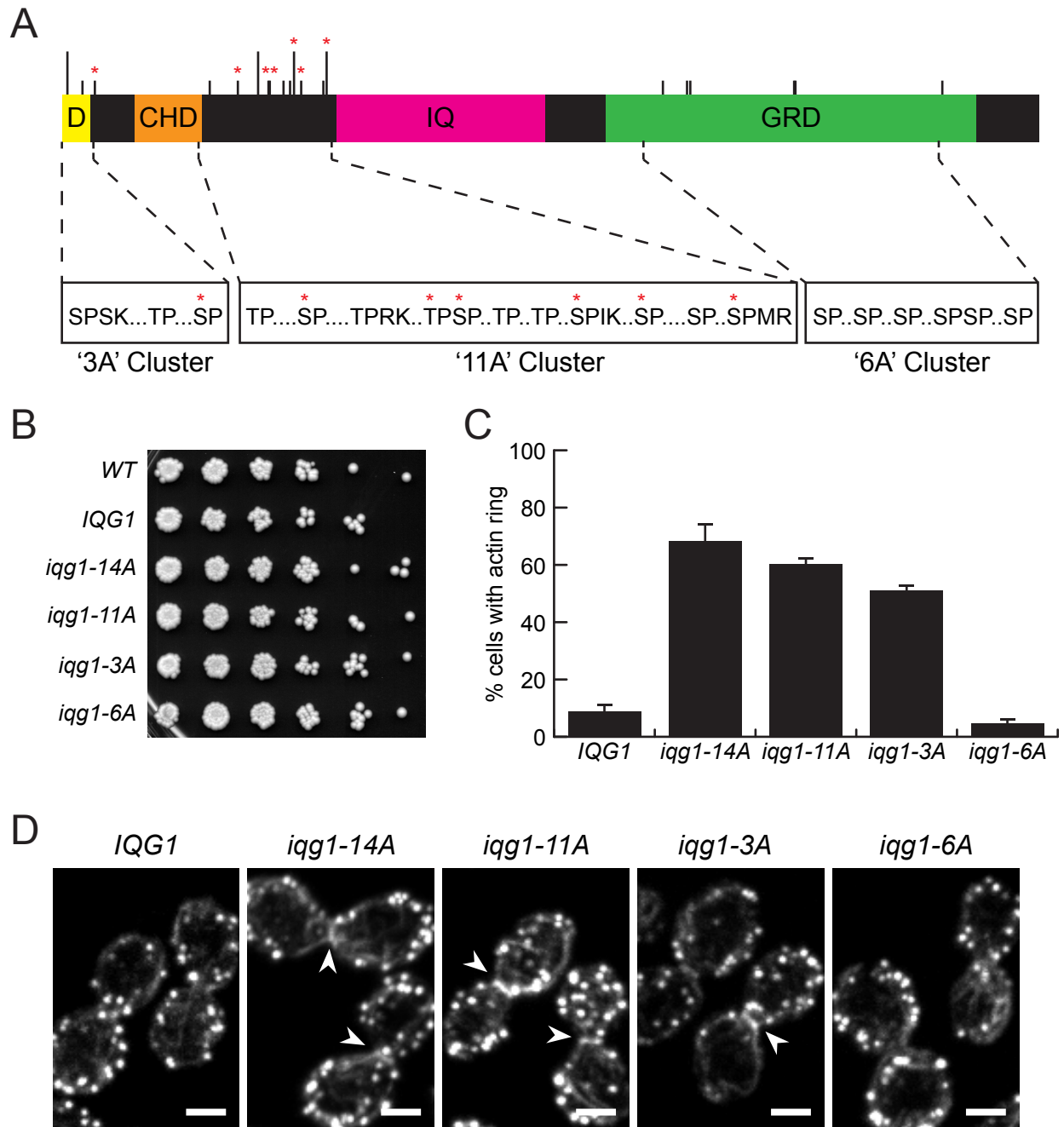
FIGURE 2

Iqg1 phosphorylation controls actin ring assembly. (A) Functional domains and Cdk1 consensus phosphorylation sites of Iqg1. D: APC/C recognition motif; CHD: calponin homology domain; IQ: eleven IQ repeats; GRD: GAP-related domain; short lines: minimal Cdk1 consensus motif (S/T-P); tall lines: full Cdk1 consensus motif (S/T-P-x-K/R); asterisks: sites identified as Cdk1-dependent phosphorylation sites *in vivo* (Holt, et al., 2009). Site clusters are named for their associated alanine-mutant alleles. (B) *iqg1* phosphomutants grow at wild-type rates. Serial dilutions of log-phase cultures grown on rich media at 30°C. (C) Actin ring frequency in nocodazole-arrested cells is increased in *iqg1* phosphomutants. *iqg1-14A* is mutated in both the '3A' and '11A' clusters. Error bars: SEM in two experimental repeats. (D) Representative nocodazole-arrested cells stained with phalloidin. Arrowheads: f-actin rings. Scale bars: 2 μm.

A

DAPI | Phalloidin-Alexa 488 | Spc42-mCherry | merge

IQG1

iqg1-14A

iqg1-11A

iqg1-3A

B

single SPB | pre-anaphase spindle
anaphase spindle

% of population

IQG1 | iqg1-14A | iqg1-11A | iqg1-3A

C

pre-anaphase spindle | anaphase spindle

% cells with actin ring

IQG1-WT | iqg1-14A | iqg1-11A | iqg1-3A
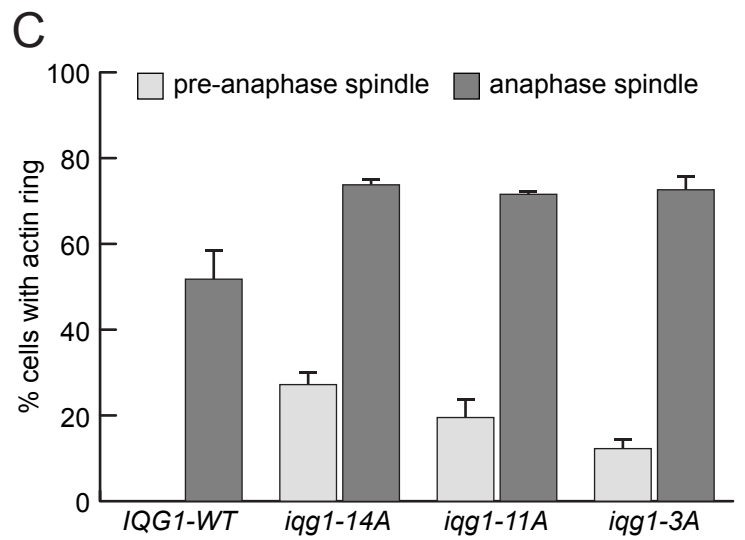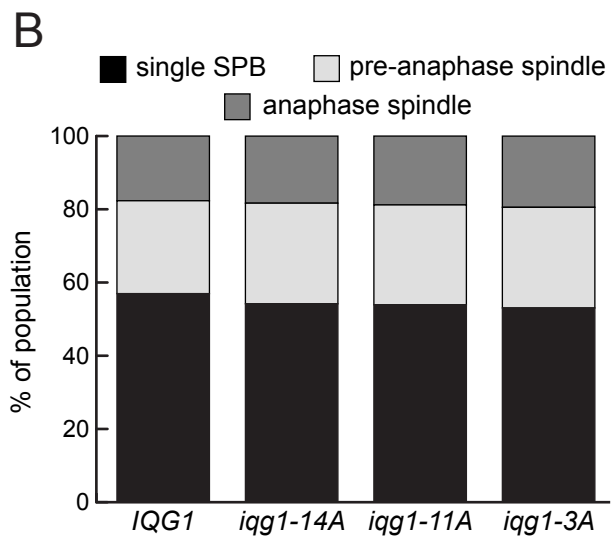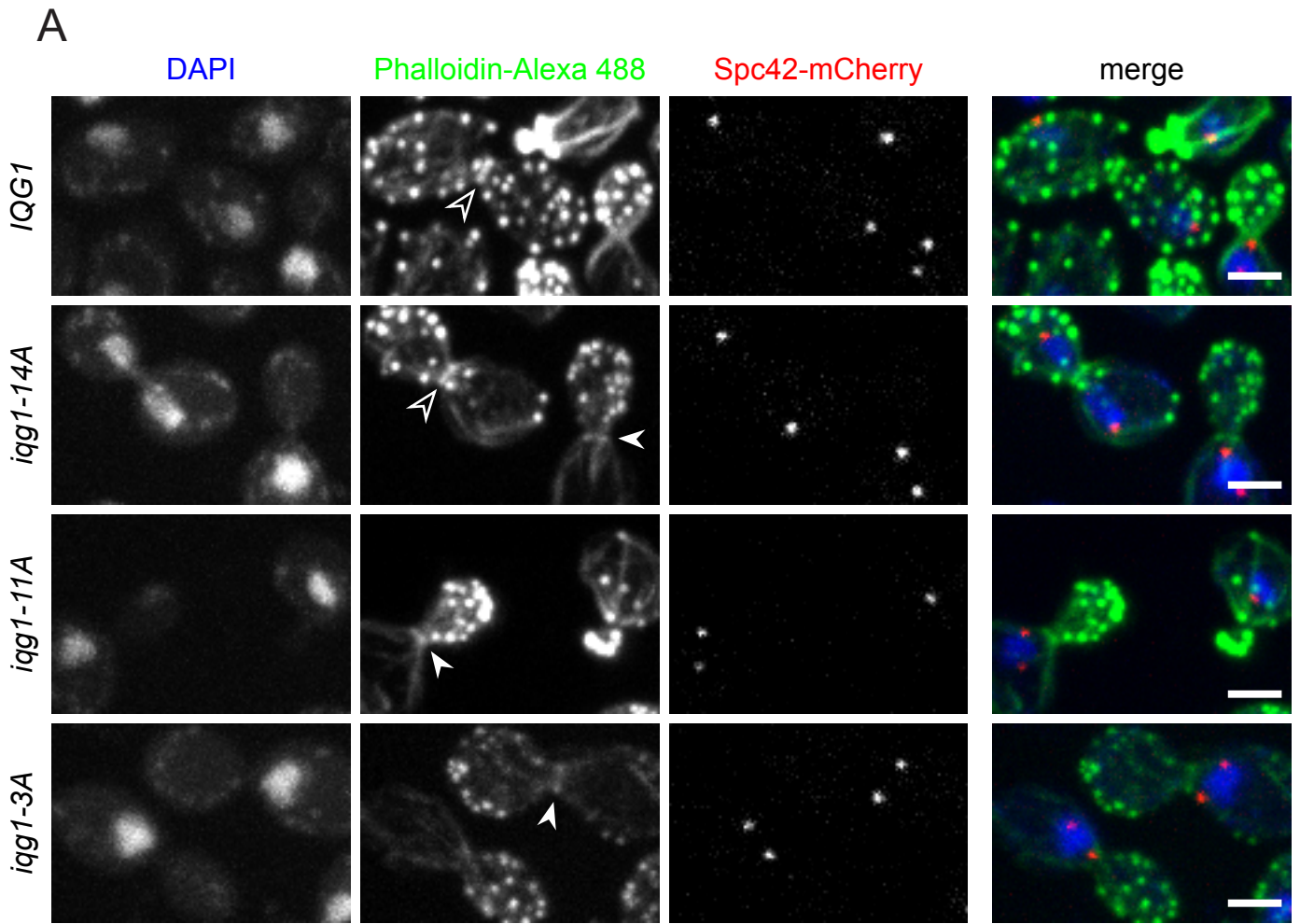
FIGURE **3**

Actin rings form prior to anaphase in *iqg1* phosphomutants. (A) Three-color imaging of cells fixed during asynchronous exponential growth. Filled arrowheads: f-actin rings in pre-anaphase cells. Open arrowheads: f-actin rings in anaphase cells. Scale bars: 2 μm. (B) Normal overall cell cycle progression in *iqg1* phosphomutants. Asynchronous cells were sorted based on DAPI and Spc42-mCherry data from part (A). "No spindle": cells with a single distinguishable SPB focus. "Pre-anaphase spindle": Cells with a single round DAPI mass and two distinguishable SPBs spaced less than 2.5 μm apart. "Anaphase spindle": Cells with an elongated or split DAPI mass and SPB spacing greater than 2.5 μm. (C) Actin ring frequency in cells of the "pre-anaphase" and "anaphase" spindle groups. No actin rings were observed in cells with a single SPB focus. Error bars: SEM in two experimental repeats.

A

IQG1   iqg1-14A

Iqg1-eGFP/Spc42-mCherry

B

C

IQG1-eGFP

iqg1-14A-eGFP

-30   -20   -10   0   10   20

Time from onset of spindle elongation (min)

D   E
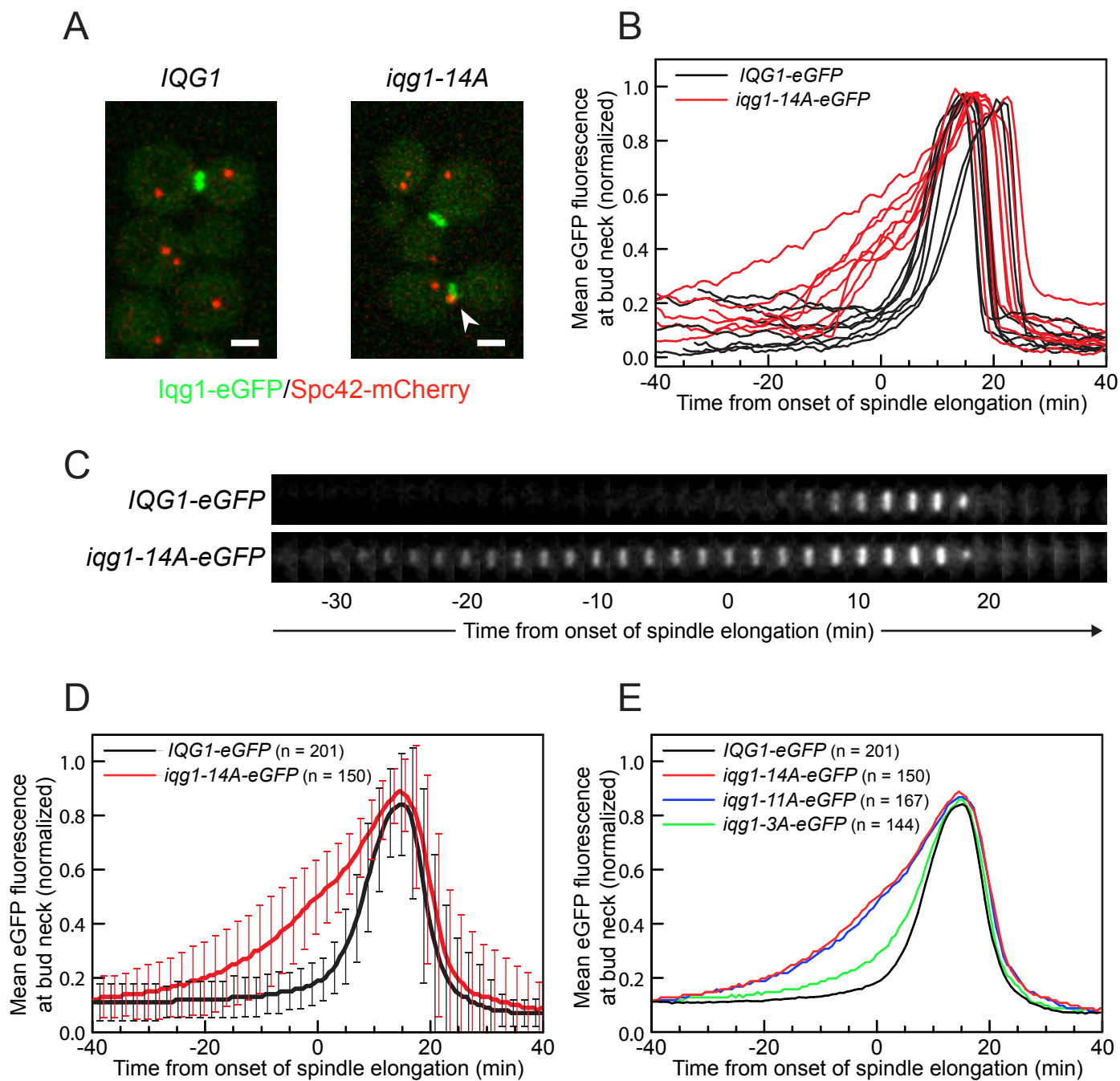
FIGURE **4**

Iqg1 phosphomutants accumulate at bud neck prematurely. (A) Live-cell images of cells expressing C-terminal fusions of *eGFP* and *mCherry* at the endogenous loci of *IQG1* and *SPC42*, respectively. Arrowhead: premature Iqg1p-eGFP accumulation at the bud neck in *iqg1* phosphomutant. Scale bars: 2 μm. (B) Quantification of green fluorescence signal in the bud neck region over time for eight representative cells from each genotype, normalized and smoothed. (C) Time series of Iqg1-eGFP dynamics at bud neck in typical wild-type and *iqg1* phosphomutant cells, two-minute intervals. Scale bar: 2 μm. (D) Population average of normalized mean eGFP fluorescence at each time point, pooling data from two experiments. Error bars: SD. (E) Population average of normalized mean eGFP fluorescence at each time point for all four *iqg1* alleles.

34

A

B

C HOF1-eGFP, IQG1

HOF1-eGFP, iqg1-14A

Time from onset of spindle elongation (min)

D
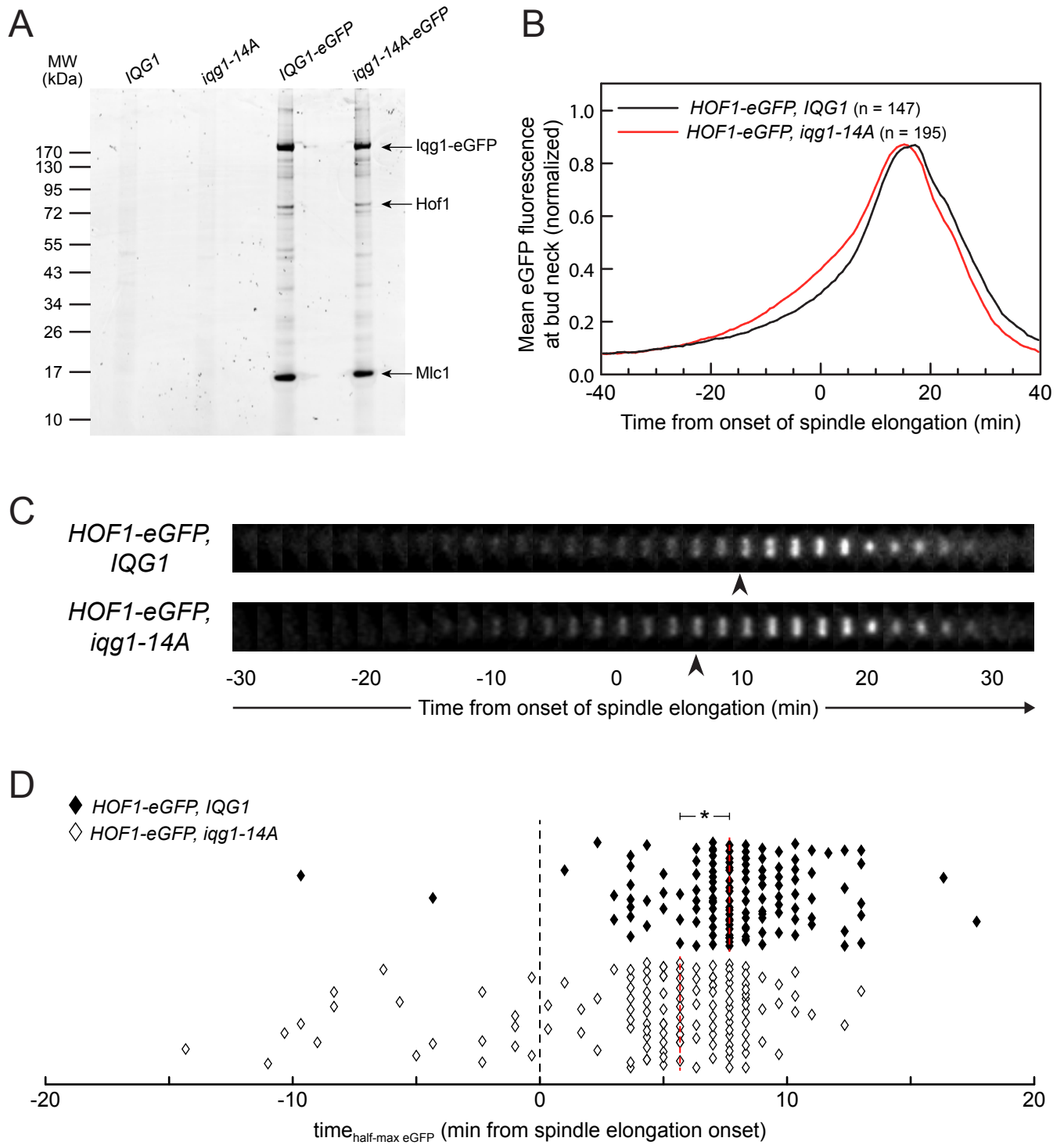
FIGURE 5

Iqg1 phosphorylation affects Hof1 bud neck accumulation. (A) Iqg1 associates with Mlc1 and Hof1 *in vivo*. Sypro-Ruby stain of Iqg1-GFP immunoprecipitates from lysates of nocodazole-arrested cells. Hof1 and Mlc1 were identified by mass spectrometry. Differences between the *IQG1-eGFP* and *iqg1-14A-eGFP* preparations were not reproduced in experimental repeats. (B) Population average of normalized mean eGFP fluorescence at each time point, pooling data from two experiments. (C) Time series of Hof1-eGFP dynamics at bud neck in typical wild-type and *iqg1-14A* cells, two-minute intervals. Scale bar: 2 μm. Arrowheads: time at which mean eGFP signal exceeds half-maximal value. (D) Distribution of time points at which a cell exceeds half-maximal Hof1p-eGFP bud neck accumulation. 133 representative cells are depicted for each population Asterisk: 2 minute difference in median values, P < 0.0004 (dual ranksum and resampling tests).

A

Mean eGFP fluorescence at bud neck (normalized)

— *CYK3-eGFP, IQG1* (n = 69)
— *CYK3-eGFP, iqg1-14A* (n = 93)

Time from onset of spindle elongation (min)

B

Mean eGFP fluorescence at bud neck (normalized)

— *INN1-eGFP, IQG1* (n = 142)
— *INN1-eGFP, iqg1-14A* (n = 96)

Time from onset of spindle elongation (min)
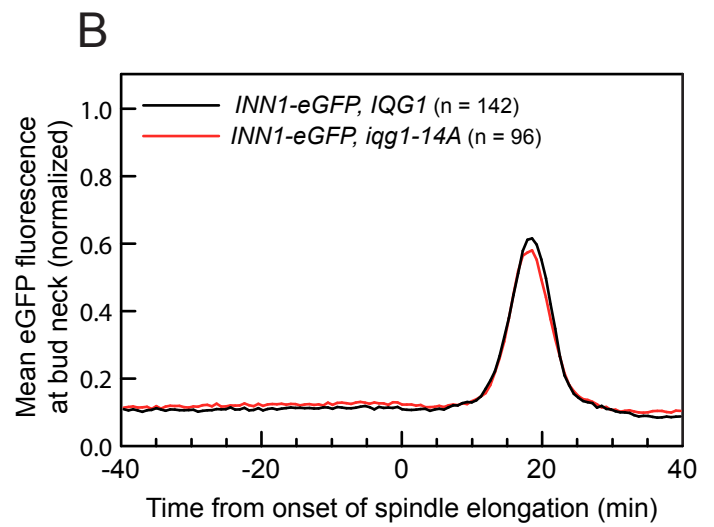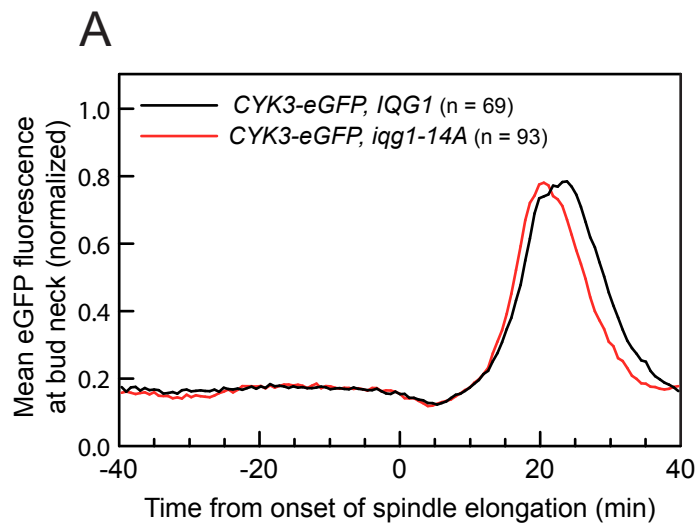
SUPPLEMENTARY FIGURE S1

Iqg1 phosphorylation does not significantly affect Cyk3 or Inn1 bud neck accumulation. (A) Cyk3-eGFP was analyzed by the same methods used for other eGFP-tagged proteins. Population average of normalized mean Cyk3-eGFP fluorescence at each time point. (B) Inn1-eGFP analyzed as in (A).

Table S1: Yeast Strains

Strain	Relevant Genotype	*iqg1* Mutations
SN001	WT background strain	WT
SN143	*cdk1-as*	WT
SN312	*IQG1, SPC42-mCherry*	WT
SN313	*iqg1-14A, SPC42-mCherry*	S7A, T30A, S49A, T225A, S268A, T299A, T315A, S317A, T338A, T348A, S354A, S365A, S399A, S404A
SN314	*iqg1-11A, SPC42-mCherry*	T225A, S268A, T299A, T315A, S317A, T338A, T348A, S354A, S365A, S399A, S404A
SN315	*iqg1-3A, SPC42-mCherry*	S7A, T30A, S49A
SN158	*iqg1-6A, SPC42-mCherry*	S919A, S956A, S961A, S1120A, S1122A, S1347A
SN320	*IQG1-eGFP, SPC42-mCherry*	WT
SN321	*iqg1-14A-eGFP, SPC42-mCherry*	S7A, T30A, S49A, T225A, S268A, T299A, T315A, S317A, T338A, T348A, S354A, S365A, S399A, S404A
SN322	*iqg1-11A-eGFP, SPC42-mCherry*	T225A, S268A, T299A, T315A, S317A, T338A, T348A, S354A, S365A, S399A, S404A
SN323	*iqg1-3A-eGFP, SPC42-mCherry*	S7A, T30A, S49A
SN324	*HOF1-eGFP, IQG1, SPC42-mCherry*	WT
SN342	*HOF1-eGFP, iqg1-14A, SPC42-mCherry*	S7A, T30A, S49A, T225A, S268A, T299A, T315A, S317A, T338A, T348A, S354A, S365A, S399A, S404A
SN326	*HOF1-eGFP, iqg1-11A, SPC42-mCherry*	T225A, S268A, T299A, T315A, S317A, T338A, T348A, S354A, S365A, S399A, S404A
SN327	*HOF1-eGFP, iqg1-3A, SPC42-mCherry*	S7A, T30A, S49A

Table S2: Plasmids

Plasmid	Source	Features
pRS306		*URA3, AmpR*
pSGN092	pRS306 + PCR	*IQG1, URA3, AmpR*
pSGN084	Invitrogen LifeTech	*iqg1-14A* (-185 – 1464)
pSGN085	Invitrogen LifeTech	*iqg1-5A* (2635 – 3544)
pSGN094	pSGN092 + pSGN085	*iqg1-6A, URA3, AmpR*
pSGN098	pSGN094 + pSGN084	*iqg1-20A, URA3, AmpR*
pSGN109	pSGN092 + pSGN098	*iqg1-11A, URA3, AmpR*
pSGN111	pSGN092 + pSGN098	*iqg1-3A, URA3, AmpR*
pYM28	PCR Toolbox II (John Pringle)	*eGFP, HIS3MX6, AmpR*
pSGN099		*mCherry, kanMX, AmpR*

Table S3A: Mass Spectrometric Analysis of Band Identified as Mlc1

Rank	# Unique Peptides	% Coverage	Protein MW (kDa)	Species	Protein Name	Systematic Name (Yeast)
1	9	53.0	16.4	*S. cerevisiae*	Mlc1	YGL106W
2	5	11.3	58.8	*H. sapiens*	Keratin I	N/A
3	5	11.5	66.0	*H. sapiens*	Keratin II	N/A
4	5	42.3	14.5	*S. cerevisiae*	Rps14A	YCR031C
5	4	25.3	15.3	*S. cerevisiae*	Rps24A	YER074W
6	2	17.0	16.1	*S. cerevisiae*	Cmd1	YBR109C
7	2	13.0	24.4	*S. scrofa*	Trypsin	N/A
8	3	28.8	17.0	*S. cerevisiae*	Rps18A	YDR045W
9	1	2.0	70.9	*M. musculus*	Keratin II	N/A
10	2	14.2	14.2	*S. cerevisiae*	Rpl26A	YLR344W
11	1	5.4	22.3	*H. brasiliensis*	Rubber	N/A
12	1	8.0	14.7	*H. brasiliensis*	Rubber EF	N/A
13	1	1.8	62.1	*H. sapiens*	Keratin I	N/A
14	2	19.2	13.9	*S. cerevisiae*	Rpl35A	YDL191W

Table S3B: Mass Spectrometric Analysis of Band Identified as Hof1

Rank	# Unique Peptides	% Coverage	Protein MW (kDa)	Species	Protein Name	Systematic Name (Yeast)
1	25	37.7	76.2	*S. cerevisiae*	Hof1	YMR032W
2	8	10.7	99.6	*S. cerevisiae*	Pma1	YGL008C
3	7	11.6	81.4	*S. cerevisiae*	Hsp82	YPL240C
4	7	4.9	172.8	*S. cerevisiae*	Iqg1	YPL242C
5	4	8.7	69.7	*S. cerevisiae*	Ssa1	YAL005C
6	2	4.1	69.3	*B. taurus*	BSA	N/A
7	2	12.1	24.4	*S. scrofa*	Trypsin	N/A
8	1	3.4	36.9	*S. cerevisiae*	Adh1	YOL086C
9	3	4.5	77.4	*S. cerevisiae*	Sse1	YPL106C
10	1	1.8	80.8	*S. cerevisiae*	Gus1	YGL245W
11	2	3.1	92.3	*S. cerevisiae*	Ubp5	YER144C
12	1	2.4	50.6	*A. salina*	EF-1-alpha	N/A
13	1	2.7	46.8	*S. cerevisiae*	Eno1	YGR254W
14	1	1.4	78.2	*S. cerevisiae*	Grs1	YBR121C
15	1	1.2	85.7	*S. cerevisiae*	Mes1	YGR264C

Visible GelCode Blue-stained protein bands were excised for in-gel trypsin digest, HPLC fractionation, and linear ion trap – Orbitrap hybrid tandem mass spectrometry. (A) Analysis of the major lower MW band identified Mlc1 (P53141) as the major component (identified from 9 unique peptides, providing 53% sequence coverage). (B) Analysis of the higher MW band identified Hof1 (Q05080) as the major component (from 25 unique peptides, providing ~38% sequence coverage). These proteins were confirmed as unique interactors with the Iqg1-eGFP bait by comparison of the full protein content of the experimental IP with that from a control IP with a strain lacking Iqg1 (data not shown).

40

CHAPTER 3: CONCLUSION

The regulation of cellular events by constitutes an informational system encoded within a set of physical interactions. There is no centralized "master code" to which the cell can refer in order to ascertain the instructions contained in the presence or state of a particular protein. Therefore, the informational content of each molecule depends entirely upon its interactions with every other molecule. While this is true for every cellular process, the cyclical nature of the cell cycle drives the point home especially effectively, as there is no identifiable starting event of which every other event can be thought of as a downstream consequence.

Cdk-dependent phosphoregulation provides an excellent model system to study how physical protein modification translates to informational organization. Every Cdk-dependent phosphate modification looks similar in broad strokes: a doubly negatively-charged PO_4 group linked via phosphodiester bond to a serine or threonine side chain on the surface of a protein, with a proline residue situated immediately toward the protein's C-terminus. Yet the ever-expanding body of research on these modifications shows that this motif can have wildly different consequences in different contexts, from the creation of a binding surface to promote interaction with a partner molecule, to the disruption of such an interaction, to a conformational change within the protein itself. The research presented in this dissertation advances the understanding of the physical/informational logic of cell cycle regulation by identifying new instances of regulatory phosphorylation, describing their cellular consequences, and providing templates for further exploration along these lines.

The most significant findings in the research presented here concern the effect of protein phosphorylation on the rate of accumulation of various budding yeast proteins at the bud neck in preparation for cytokinesis. These findings were made possible by advances in quantitative confocal fluorescence microscopy, a technology that now permits relative measurements of tagged protein concentration in a three-dimensional region with considerable precision. The finding that Hof1 begins accumulation early without the inhibitory effect of Cdk-phosphorylated Iqg1 would not have been demonstrably significant had we relied on simple visual assessment of Hof1-GFP data. Quantitative microscopy also revealed that the onset of Iqg1 bud neck localization and the completion of that localization are apparently regulated by separate means, as the Iqg1 phosphomutant dramatically altered the slope of the first half of the Iqg1-GFP accumulation curve but did not affect the timing nor the intensity of the peak of that accumulation just prior to cytokinesis.

The above findings are meaningful not only for what they tell us about the particular proteins involved, but because they help open the world of cell cycle research to more subtle study of the scalable forms of regulation involved in most processes. Much of the best work in cell cycle research has concerned the cell's impressive talent for evolving biphasic, switch-like transitions. Examples include the promotion of a sudden G1-S switch by the multi-step phosphorylation of Cdk inhibitor Sic1[56, 57], the enzymatic processivity of the APC/C ubiquitin ligase that ensures rapid and complete degradation of its protein substrates[58, 59], the coordination of positive feedback loops between phosphorylation and ubiquitination[60], and the systems-level modeling of switch-like behavior at the metaphase-anaphase transition[61, 62]. In each of these examples, the cell

attains a clear benefit in reproductive viability by keeping the process in question as close as possible to a binary moment, minimizing the probability of catastrophes such as chromosome mis-segregation and imperfect duplication of the genome.

Between these nearly binary moments, however, are equally essential processes that necessarily proceed with finite, scalable rates, and these rates are themselves the product of evolved regulation. This regulation has received less productive study for a few reasons. For one, the rigors of statistical analysis and the demands of competitive publication make it much easier to demonstrate a biologically significant effect when that effect involves disruption of an all-or-none event. For another, our broader social context of working within the Age of Information conditions us to understand biological systems by comparison to digital computational systems, so that all meaningful transmission of information must occur by approximating the gates and switches of a microprocessor, with the cell doing the best it can to get its macromolecular lumps of clay to behave like the more perfect silicons and rare earth metals at the material heart of the digital world.

The trouble with such a conceptual framework is that it fails to recognize the additional opportunities for fine-tuned regulation afforded by the analog control of the scalable aspects of cellular processes. The broadening of the Iqg1-GFP accumulation curve in response to phosphomutagenesis is on the one hand another clear example of an evolved mechanism for producing a switch-like transition, with the cell exploiting the wave of anaphase dephosphorylation activity to minimize the time between a bud neck with no Iqg1/actin and a bud neck with all the Iqg1/actin it needs. But on the other hand, comparison of the various protein accumulation curves produced by this study raises questions about why (and how) those curves take the exact shape they do. Why does

Hof1 begin accumulation earlier and more gradually than Iqg1, but also respond in a downstream manner to changes in the latter? Would it really be most optimal if the cell could accumulate all of the relevant proteins—Iqg1, Hof1, Cyk3, Inn1, actin and others—instantaneously and in precise order, or does the complex structural geometry of the dual-functional septation apparatus benefit from a more intermingled pattern of accumulation and mutual recruitment dependencies? These are the questions that this study begins to address, and additional proteins should be mutated and quantitatively observed to help address and answer them further.

Similar quantitative microscopy techniques are also producing findings of interest elsewhere in the cell cycle. The metaphase-anaphase transition is perhaps the most striking illustration of switch-like behavior in all of biology, with sister chromatids springing apart from one another in near perfect synchrony thanks to a complex regulatory system involving ubiquitin-mediated degradation of the enzyme inhibitor securin and the subsequent elimination of sister chromatid cohesion caused by proteolysis of the cohesin complex by the enzyme separase, with phosphorylation also influencing each of the proteins involved. Quantitative monitoring of these components, three-dimensional tracking of chromosomal movements, and development of microscopy-based biosensors of localized enzyme activity have all contributed to a deeper understanding of the underlying processes whose scalar parameters facilitate the switch[63, 64]. Current areas of inquiry included the question of exactly how much securin must be degraded to yield an active separase population, and exactly how many cohesin molecules along a chromosome pair must be cleaved to allow chromatids to separate under the force of depolymerizing microtubules.

Another area in which scalar values may contain regulatory information is in the interactions between enzyme and substrate. Unpublished research done in the service of this dissertation concerned the differential rates of catalysis of the cell cycle phosphatase Cdc14 toward its various Cdk-phosphorylated substrates, and the role that those differences might play in determining the order of population-level substrate dephosphorylation during anaphase, an important factor in the progression of mitotic exit [65]. This research was abandoned without conclusive results for technical reasons, but an independent research group completed a similar study, and indeed found, within a small sample of three Cdc14 substrates, a strong correlation between the phosphoproteins' rates of *in vitro* dephosphorylation by Cdc14 and the timing of their bulk dephosphorylation following the release of active Cdc14 during the metaphase-anaphase transition[66]. If such a correlation were to hold over a larger sample of substrates, it would suggest that subtle regulatory information is meaningfully encoded within the particulars of an enzyme-substrate interaction, suggesting that an optimally evolved regulatory enzyme is not necessarily one that has maximized its efficiency of catalysis toward every one of its substrates. Further study along these lines should include attempts to identify determining features of primary or higher-order structure that determine a substrate's susceptibility or resistance to dephosphorylation by Cdc14, as well as usage of temporally precise mass spectrometric evaluation of the phosphoproteome throughout anaphase using methods known to be effective in identification of Cdk-dependent phosphorylation[48].

The emergence from simple chemical elements of the endlessly varied and adaptable phenomena collectively known as Life is a miracle of organized information far beyond any other found in the known universe. Complexity appears at every scale of

magnification, and we find vital information within that complexity at every scale of analysis. Any biological feature that appears reducible to something like a yes/no logic gate contains, if one looks more closely, scalable and measurable properties within it. Any process whose progress over time might be approximated using a graph with right angles and a vertical line actually has rounded corners. A biological system can never be fully reduced to a digitally encoded packet of information, and to bridge the gap in understanding between chemical knowledge and biological knowledge is a task without possibility of completion.

This should make conductors of basic research in the natural sciences rejoice with optimism. We will never run out of chances to make that next discovery that will unlock untold applications, opportunities to manipulate the wild of nature for the increased welfare of human beings and of the world. And we will never run out of ways to stimulate the unique thrill of scientific understanding, the chance to color in one more doodled filigree in the baroque sprawl of creation's mystery.

BIBLIOGRAPHY

1. Morgan, D. O. The Cell Cycle: Principles of Control (New Science Press, London, 2007).

2. Hershko, A. & Ciechanover, A. The ubiquitin system. Annu Rev Biochem 67, 425-79 (1998).

3. Satterwhite, L. L. & Pollard, T. D. Cytokinesis. Curr Opin Cell Biol 4, 43-52 (1992).

4. Mabuchi, I. Cleavage furrow: timing of emergence of contractile ring actin filaments and establishment of the contractile ring by filament bundling in sea urchin eggs. J Cell Sci 107 (Pt 7), 1853-62 (1994).

5. Wloka, C. & Bi, E. Mechanisms of cytokinesis in budding yeast. Cytoskeleton (Hoboken) 69, 710-26 (2012).

6. Bi, E. et al. Involvement of an actomyosin contractile ring in Saccharomyces cerevisiae cytokinesis. The Journal of Cell Biology 142, 1301-12 (1998).

7. Bi, E. & Park, H.-O. Cell polarization and cytokinesis in budding yeast. Genetics 191, 347-87 (2012).

8. Lippincott, J. & Li, R. Sequential assembly of myosin II, an IQGAP-like protein, and filamentous actin to a ring structure involved in budding yeast cytokinesis. The Journal of Cell Biology 140, 355-66 (1998).

9. Rodriguez, J. R. & Paterson, B. M. Yeast myosin heavy chain mutant: maintenance of the cell type specific budding pattern and the normal deposition of

chitin and cell wall components requires an intact myosin heavy chain gene. Cell Motil Cytoskeleton 17, 301-8 (1990).

10.   Schmidt, M., Bowers, B., Varma, A., Roh, D.-H. & Cabib, E. In budding yeast, contraction of the actomyosin ring and formation of the primary septum at cytokinesis depend on each other. Journal of Cell Science 115, 293-302 (2002).

11.   Pringle, J. R. et al. Establishment of cell polarity in yeast. Cold Spring Harb Symp Quant Biol 60, 729-44 (1995).

12.   Drubin, D. G. & Nelson, W. J. Origins of cell polarity. Cell 84, 335-44 (1996).

13.   Lee, P. R. et al. Bni5p, a septin-interacting protein, is required for normal septin function and cytokinesis in Saccharomyces cerevisiae. Mol Cell Biol 22, 6906-20 (2002).

14.   Vallen, E. A., Caviston, J. & Bi, E. Roles of Hof1p, Bni1p, Bnr1p, and myo1p in cytokinesis in Saccharomyces cerevisiae. Molecular Biology of the Cell 11, 593-611 (2000).

15.   Fang, X. et al. Biphasic targeting and cleavage furrow ingression directed by the tail of a myosin II. The Journal of Cell Biology 191, 1333-50 (2010).

16.   Boyne, J. R., Yosuf, H. M., Bieganowski, P., Brenner, C. & Price, C. Yeast myosin light chain, Mlc1p, interacts with both IQGAP and class II myosin to effect cytokinesis. Journal of Cell Science 113 Pt 24, 4533-43 (2000).

17.   Shannon, K. B. & Li, R. A myosin light chain mediates the localization of the budding yeast IQGAP-like protein during contractile ring formation. Curr Biol 10, 727-30 (2000).

18. Epp, J. A. & Chant, J. An IQGAP-related protein controls actin-ring formation and cytokinesis in yeast. Curr Biol 7, 921-9 (1997).

19. Shannon, K. B. & Li, R. The multiple roles of Cyk1p in the assembly and function of the actomyosin ring in budding yeast. Molecular Biology of the Cell 10, 283-96 (1999).

20. Sburlati, A. & Cabib, E. Chitin synthetase 2, a presumptive participant in septum formation in Saccharomyces cerevisiae. J Biol Chem 261, 15147-52 (1986).

21. Shaw, J. A. et al. The function of chitin synthases 2 and 3 in the Saccharomyces cerevisiae cell cycle. The Journal of Cell Biology 114, 111-23 (1991).

22. Kamei, T. et al. Interaction of Bnr1p with a novel Src homology 3 domain-containing Hof1p. Implication in cytokinesis in Saccharomyces cerevisiae. J Biol Chem 273, 28341-5 (1998).

23. Lippincott, J. & Li, R. Dual function of Cyk2, a cdc15/PSTPIP family protein, in regulating actomyosin ring dynamics and septin distribution. The Journal of Cell Biology 143, 1947-60 (1998).

24. Korinek, W. S. et al. Cyk3, a novel SH3-domain protein, affects cytokinesis in yeast. Curr Biol 10, 947-50 (2000).

25. Sanchez-Diaz, A. et al. Inn1 couples contraction of the actomyosin ring to membrane ingression during cytokinesis in budding yeast. Nat Cell Biol 10, 395-406 (2008).

26. Nishihama, R. et al. Role of Inn1 and its interactions with Hof1 and Cyk3 in promoting cleavage furrow and septum formation in S. cerevisiae. The Journal of Cell Biology 185, 995-1012 (2009).

27.   VerPlank, L. & Li, R. Cell cycle-regulated trafficking of Chs2 controls actomyosin ring stability during cytokinesis. Molecular Biology of the Cell 16, 2529-43 (2005).

28.   Roh, D.-H., Bowers, B., Schmidt, M. & Cabib, E. The septation apparatus, an autonomous system in budding yeast. Molecular Biology of the Cell 13, 2747-59 (2002).

29.   Jendretzki, A., Ciklic, I., Rodicio, R., Schmitz, H.-P. & Heinisch, J. J. Cyk3 acts in actomyosin ring independent cytokinesis by recruiting Inn1 to the yeast bud neck. Mol Genet Genomics 282, 437-51 (2009).

30.   Meitinger, F. et al. Targeted localization of Inn1, Cyk3 and Chs2 by the mitotic-exit network regulates cytokinesis in budding yeast. Journal of Cell Science 123, 1851-61 (2010).

31.   Bashour, A. M., Fullerton, A. T., Hart, M. J. & Bloom, G. S. IQGAP1, a Rac- and Cdc42-binding protein, directly binds and cross-links microfilaments. The Journal of Cell Biology 137, 1555-66 (1997).

32.   Fukata, M. et al. Regulation of cross-linking of actin filament by IQGAP1, a target for Cdc42. J Biol Chem 272, 29579-83 (1997).

33.   White, C. D., Erdemir, H. H. & Sacks, D. B. IQGAP1 and its binding proteins control diverse biological functions. Cell Signal 24, 826-34.

34.   Hart, M. J., Callow, M. G., Souza, B. & Polakis, P. IQGAP1, a calmodulin-binding protein with a rasGAP-related domain, is a potential effector for cdc42Hs. Embo J 15, 2997-3005 (1996).

35.   Stegmeier, F. & Amon, A. Closing mitosis: the functions of the Cdc14 phosphatase and its regulation. Annu. Rev. Genet. 38, 203-32 (2004).

36.   Mishima, M., Pavicic, V., Grüneberg, U., Nigg, E. A. & Glotzer, M. Cell cycle regulation of central spindle assembly. Nature 430, 908-13 (2004).

37.   Khmelinskii, A., Roostalu, J., Roque, H., Antony, C. & Schiebel, E. Phosphorylation-dependent protein interactions at the spindle midzone mediate cell cycle regulation of spindle elongation. Developmental Cell 17, 244-56 (2009).

38.   Sullivan, M., Holt, L. & Morgan, D. O. Cyclin-specific control of ribosomal DNA segregation. Molecular and Cellular Biology 28, 5328-36 (2008).

39.   Teh, E. M., Chai, C. C. & Yeong, F. M. Retention of Chs2p in the ER requires N-terminal CDK1-phosphorylation sites. Cell Cycle 8, 2964-74 (2009).

40.   Chin, C. F., Bennett, A. M., Ma, W. K., Hall, M. C. & Yeong, F. M. Dependence of Chs2 ER export on dephosphorylation by cytoplasmic Cdc14 ensures that septum formation follows mitosis. Molecular Biology of the Cell 23, 45-58 (2012).

41.   Bloom, J. et al. Global analysis of Cdc14 phosphatase reveals diverse roles in mitotic processes. J Biol Chem 286, 5434-45 (2011).

42.   Cid, V. J., Adamiková, L., Sánchez, M., Molina, M. & Nombela, C. Cell cycle control of septin ring dynamics in the budding yeast. Microbiology (Reading, Engl) 147, 1437-50 (2001).

43.   Lippincott, J., Shannon, K. B., Shou, W., Deshaies, R. J. & Li, R. The Tem1 small GTPase controls actomyosin and septin dynamics during cytokinesis. J Cell Sci 114, 1379-86 (2001).

44.   Sanchez-Diaz, A., Nkosi, P. J., Murray, S. & Labib, K. The Mitotic Exit Network and Cdc14 phosphatase initiate cytokinesis by counteracting CDK phosphorylations and blocking polarised growth. The EMBO Journal 31, 3620-34 (2012).

45.   Luca, F. C. et al. Saccharomyces cerevisiae Mob1p is required for cytokinesis and mitotic exit. Molecular and Cellular Biology 21, 6972-83 (2001).

46.   Niiya, F., Xie, X., Lee, K. S., Inoue, H. & Miki, T. Inhibition of cyclin-dependent kinase 1 induces cytokinesis without chromosome segregation in an ECT2 and MgcRacGAP-dependent manner. J Biol Chem 280, 36502-9 (2005).

47.   Bishop, A. C. et al. A chemical switch for inhibitor-sensitive alleles of any protein kinase. Nature 407, 395-401 (2000).

48.   Holt, L. J. et al. Global analysis of Cdk1 substrate phosphorylation sites provides insights into evolution. Science 325, 1682-6 (2009).

49.   Li, C. R., Wang, Y. M. & Wang, Y. The IQGAP Iqg1 is a regulatory target of CDK for cytokinesis in Candida albicans. Embo J 27, 2998-3010 (2008).

50.   Ko, N. et al. Identification of yeast IQGAP (Iqg1p) as an anaphase-promoting-complex substrate and its role in actomyosin-ring-independent cytokinesis. Molecular Biology of the Cell 18, 5139-53 (2007).

51.   Tully, G. H., Nishihama, R., Pringle, J. R. & Morgan, D. O. The anaphase-
        promoting complex promotes actomyosin-ring disassembly during cytokinesis in
        yeast. Molecular Biology of the Cell 20, 1201-12 (2009).

52.   Mateer, S. C., Morris, L. E., Cromer, D. A., Bensenor, L. B. & Bloom, G. S.
        Actin filament binding by a monomeric IQGAP1 fragment with a single calponin
        homology domain. Cell Motil Cytoskeleton 58, 231-41 (2004).

53.   Oh, Y., Schreiter, J., Nishihama, R., Wloka, C. & Bi, E. Targeting and functional
        mechanisms of the cytokinesis-related F-BAR protein Hof1 during the cell cycle.
        Mol Biol Cell 24, 1305-20 (2013).

54.   Bi, E. Cytokinesis in budding yeast: the relationship between actomyosin ring
        function and septum formation. Cell Struct Funct 26, 529-37 (2001).

55.   Edelstein, A., Amodaj, N., Hoover, K., Vale, R. & Stuurman, N. Computer
        control of microscopes using microManager. Curr Protoc Mol Biol Chapter 14,
        Unit14 20.

56.   Nash, P. et al. Multisite phosphorylation of a CDK inhibitor sets a threshold for
        the onset of DNA replication. Nature 414, 514-21 (2001).

57.   Koivomagi, M. et al. Cascades of multisite phosphorylation control Sic1
        destruction at the onset of S phase. Nature 480, 128-31.

58.   Rodrigo-Brenni, M. C. & Morgan, D. O. Sequential E2s drive polyubiquitin chain
        assembly on APC targets. Cell 130, 127-39 (2007).

59.   Matyskiela, M. E., Rodrigo-Brenni, M. C. & Morgan, D. O. Mechanisms of
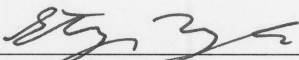   ubiquitin transfer by the anaphase-promoting complex. J Biol 8, 92 (2009).

60.   Holt, L. J., Krutchinsky, A. N. & Morgan, D. O. Positive feedback sharpens the anaphase switch. Nature 454, 353-7 (2008).

61.   Toth, A., Queralt, E., Uhlmann, F. & Novak, B. Mitotic exit in two dimensions. J Theor Biol 248, 560-73 (2007).

62.   Drapkin, B. J., Lu, Y., Procko, A. L., Timney, B. L. & Cross, F. R. Analysis of the mitotic exit control system using locked levels of stable mitotic cyclin. Mol Syst Biol 5, 328 (2009).

63.   Yaakov, G., Thorn, K. & Morgan, D. O. Separase biosensor reveals that cohesin cleavage timing depends on phosphatase PP2A(Cdc55) regulation. Dev Cell 23, 124-36.

64.   Lu, D. & Morgan, D. O. Unpublished data. (2013).

65.   Sullivan, M. & Morgan, D. O. Finishing mitosis, one step at a time. Nat Rev Mol Cell Biol 8, 894-903 (2007).

66.   Bouchoux, C. & Uhlmann, F. A quantitative model for ordered Cdk substrate dephosphorylation during mitotic exit. Cell 147, 803-14 (2011).

54

Publishing Agreement

It is the policy of the University to encourage the distribution of all theses, dissertations, and manuscripts. Copies of all UCSF theses, dissertations, and manuscripts will be routed to the library via the Graduate Division. The library will make all theses, dissertations, and manuscripts accessible to the public and will preserve these to the best of their abilities, in perpetuity.

Please sign the following statement:

I hereby grant permission to the Graduate Division of the University of California, San Francisco to release copies of my thesis, dissertation, or manuscript to the Campus Library to provide access and preservation, in whole or in part, in perpetuity.

_____   20 Sep 2013
Author Signature   Date